CHEOPS AOCS IN-FLIGHT EXPERIENCE

Amador López-Pina [1], Alberto Pizarro [1] Laura Torres[1]
Carlos Corral [2], Andrew Hyslop [2]

[1] AIRBUS Defence & Space –Getafe (Madrid), Spain
amador.lopez@airbus.com;alberto.lopez@airbus.com;laura.torres@airbus.com
[2] ESA-ESTEC – Noordwijk, The Netherlands
carlos.corral.van.damme@esa.int; andrew.hyslop@esa.int

ABSTRACT

CHEOPS (CHaracterizing ExoPlanet Satellite) is the first mission dedicated to search for transits of exoplanets using ultrahigh precision photometry on bright stars already known to host planets. It is the first S-class (small) mission in the ESA Science Programme, and it has been implemented by means of a partnership with Switzerland, which among other tasks was in charge of scientific lead and instrument development. Airbus Defence and Space Spain has been the prime designer and manufacturer of the platform, also conducting the satellite design, integration, validation and test. Finally, Airbus has been responsible to lead and execute the LEOP and IOC activities and has also acted as Mission Control System provider.

CHEOPS was successfully launched from Kourou on December 18th, 2019 as a secondary passenger embarked on a Soyuz launcher. At the end of the in-orbit commissioning, the spacecraft started its nominal 3.5 years mission. The platform is based on AS250 product line from Airbus, which has been adapted to a scientific mission (a goal different from Earth Observation, which is the aim of this product line). The AOCS features a gyroless solution and it implements a payload in the loop design. The pointing performances highly improve the required APE of 4 arcseconds at 68%, reaching values below 1 arcsecond. Considering the mission needs, the design of the platform does not embark a GPS receiver, and orbit determination is based on Doppler measurements, which allows estimating the orbit on ground. The state vector is periodically and automatically uplinked from ground and subsequently propagated onboard. Besides review of achieved performances, this paper details in orbit experience for payload in the loop behaviour for non-standard phases like visited star atmospheric Line of Sight passes close to Earth observation and the update of the time management to work without GPS measurements. Based on the high scientific return of the mission and the excellent performance (including AOCS behaviour), CHEOPS lifetime has been extended, potentially up to 2028.

1 INTRODUCTION

1.1 CHEOPS mission

In March 2012, the European Space Agency (ESA) issued a call for a new class of mission (S-class) in the portfolio of the science programme, and the CHEOPS (CHaracterising ExOPlanet Satellite) proposal was selected in November 2012 by ESAs Space Programme Committee among 26 competing submissions. CHEOPS mission is dedicated to the search of exoplanetary transits by

performing ultra-high precision photometry on bright stars already known to host planets. The mission addresses the demands raised within the scientific community dedicated to exoplanets research, in line with previous missions like Kepler or Corot. Following the discovery in 1995 of the first exoplanet orbiting a solar-like star and the subsequent detection of over 4000 additional planets, the need for physical and chemical characterisation of these objects has been growing in the last decades. On this regard, a sample as large as possible of planets orbiting bright stars and for which mass and radius are precisely measured is of extraordinary relevance, and CHEOPS is in charge of such extensive characterization [1]. The typical science observation is based on a "star visit" which implies the acquisition of the light coming from a selected host star, and the characterization of the decrease of incoming light when a transit of an exoplanet orbiting around it slightly occults part of the star. The phenomenon depends on the particular nature of the exoplanet and thus it allows its characterization, including the determination of its radius and orbit features. The duration of such procedure depends on the characteristics of the stars and the exoplanets and their orbits. These visits are conducted for many targets whose selection is proposed by the scientific community.

The development of the spacecraft entailed the participation of a consortium in charge of the instrument which was led by the University of Bern, while the platform has been designed and manufactured by Airbus Defence and Space Madrid [2]. The payload consists of a single instrument, namely a high performing photometer measuring light variations of target stars to ultra-high precision. On the other hand, the platform is based on the AS250 platform from Airbus, adapted to CHEOPS in order to account for its particular requirements along with the budget constraints of an S-class mission. Other key participants for the mission have been involved in the ground segment: INTA (Spain) has conducted the activities related to the Mission Operation Center (MOC), whilst the University of Genève was in charge of the Science Operation Center (SOC). Airbus Defence and Space has led the Launch and Early Orbit Phase (LEOP) and In Orbit Commissioning (IOC) task along with the provision of the MOC.

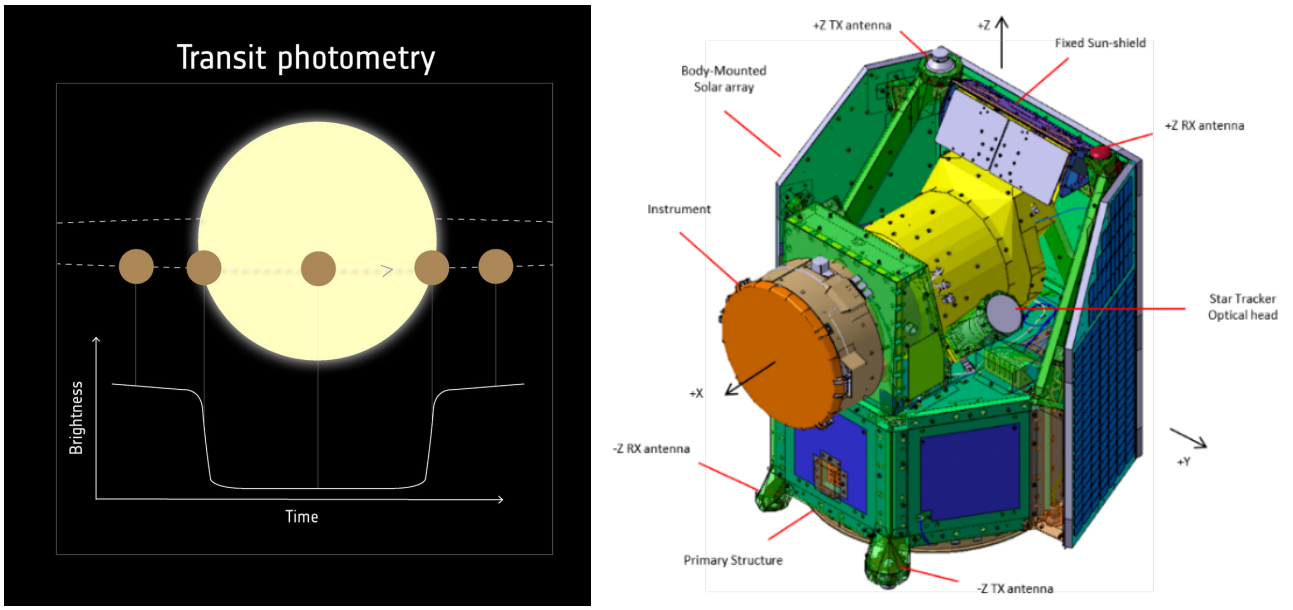

Figure 1. CHEOPS observation principle (left) and spacecraft design (right)

The spacecraft was launched on 18 December 2019 from Kourou, French Guyana, as a secondary passenger on a Soyuz-Fregat rocket. Commissioning ended in March 2020 demonstrating that

CHEOPS met all the requirements, after which the science phase subsequently followed. CHEOPS has not only achieved all the technical requirements but also the programmatic ones including the overall cost and schedule.

The spacecraft has a mass of less than 300 kg and a height of 1.5 meters. The CHEOPS mission is designed to operate from a dawn-dusk, Sun-synchronous orbit, at an altitude of 700 km. This orbit was selected during the assessment phase to maximise sky accessibility, to minimise stray-light, and to reduce the radiation environment while ensuring the largest possible number of shared launch opportunities as well as compatibility with existing platforms, qualified for Low Earth Orbit (LEO). The nominal mission design lifetime is 3.5 years, that is being currently reached, and it has been recently extended (potentially up to 2028). Almost no consumables are used for nominal operations and therefore the dominant factors limiting the lifetime of the mission are considered to be linked to radiation damage to the detector as well as overall component degradation due to exposure to cosmic radiation and ageing in general.

1.2 AOCS design summary

As previously commented, CHEOPS platform is based on the AS250 product from Airbus that has been successfully used on other missions such as Sentinel-5P, SPOT-6 and SPOT-7. The platform includes a compact, mono-propellant propulsion module, required to perform an initial launcher dispersion manoeuvre, to enable collision avoidance manoeuvres and to comply with the space debris mitigation regulations, re-entering the spacecraft within less than 25 years from the end of operations. The structure consists of a hexagonal prism, with the propulsion module accommodated next to the launcher interface. The instrument is on the top floor, where the star tracker's two optical heads are located (close to the payload focal plane to minimize effect of thermoelastic deformations) and the fixed solar arrays are oriented opposite to the instrument Line of Sight, so that the line of observation is away from the Sun, with an exclusion angle from the target star to the Sun of at least 120º. Therefore, the potential pointing envelope consists of a cone of 60º angle at each time. Considering the Earth motion around the Sun, this allows a high coverage of the sky for star visits.

Along with the rest of the platform, the AOCS has been adapted to the specific features of CHEOPS [3]. Besides the mentioned star tracker (multi-head HYDRA from SODERN), the AOCS sensors include two magnetometers in cold redundancy for safe mode. In order to reduce overall cost, the spacecraft does not include a GPS receiver, based on the low demanding needs in terms of orbit determination, which can be conducted purely based on radial velocity measurement by means of a two-way Doppler method, relying on the on-ground antenna and the redounded two spacecraft's S-band transponders. The time correlation procedure is further detailed in section §5.

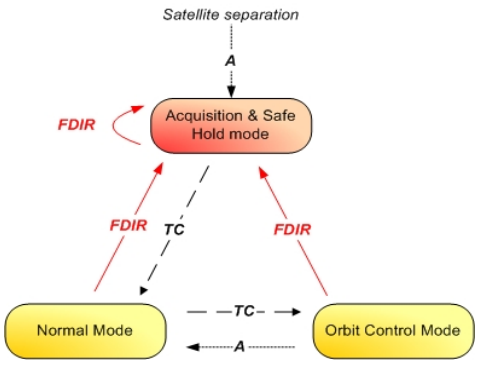

UNIT	NUMBER / REDUNDANCY	ASH	NM	OCM
Star Tracker	2 optical heads / Hot 2 electronic units / Cold	N	Y	Y
Magnetometer	2 three axes units / Cold	Y	N	N
Reaction Wheel	4 units / hot (3 out of 4)	Y	Y	Y
Magnetorquer	3 internally redounded / Cold	Y	Y	Y
Thursters	4 units / Hot (2 out of 4)	N	N	Y
Instrument TM	2 channel TM / Cold	N	Y	N

Figure 2. AOCS modes (left) and equipment use and redundancy (right)

The AOCS actuators are the three magnetorquers manufactured by ZARM (with internal coil redundancy) and four reaction wheels from MSCI, providing a torque capacity of 30 mNm and maximum angular momentum of 1.1 Nms. Furthermore, the AOCS controls the four 1-Newton thrusters of the propulsion module which are only used for orbit control manoeuvres.

The AOCS includes three modes:

- Acquisition and Safe Hold Mode (ASH) is used after launch and in case of relevant anomalies detected by the FDIR that lead to a reconfiguration. This mode uses Bdot control, with the wheels providing additional gyroscopic stabilisation about the orbit-normal axis (Sun-safe attitude).
- Normal Mode (NM) is used during most of the mission for precise inertial pointing and slew manoeuvres between target stars.
- Orbit Control Mode (OCM) is used for orbit manoeuvres.

Another adaptation of the inherited design for CHEOPS mission is the use of the instrument telemetry (TM) by the AOCS algorithms. The payload periodically provides measurements of the observed star centroid, with a rate between 1 and 1/60 Hz, and accuracy better than 1 arcsecond with a 68% confidence level (temporal statistical interpretation). This information is used by the platform software to improve the pointing performances, by estimating the bias between the payload Line of Sight and the star tracker reference frame. This bias is typically caused by low frequency thermoelastic deformations due to the evolution of the external environment which varies along the orbit and between target directions. The bias compensation allows improving the attitude estimation and consequently the final Absolute Performance Error (APE).

Airbus Defence and Space has developed the algorithms for this improvement based on applicable experience of previous projects. The AOCS development allows the use of a Dynamic-Stellar Estimator (DSE) if payload measurements are not available (as it is the case outside observations, or during observations with instrument line of sight occultations by the Earth) or alternatively of a Payload Stellar Estimator (PSE) when the instrument telemetry is used to compensate for observed bias, allowing an improvement in performances. When the system uses available instrument measurements, we will refer herein as PITL (Payload In The Loop).

2 IN ORBIT AOCS PERFORMANCE

2.1 Overall behaviour

The AOCS subsystem for CHEOPS has performed in all phases as expected. ASH mode has properly stabilized the spacecraft after launch and also for the few cases in which a spacecraft reconfiguration has been needed, with a short time of recovery in less than one orbit. Similarly, the normal mode has shown to meet the expected performances in terms of slews, attitude estimation and pointing, wheels offloading, etc. Details on pointing performances are shown in §2.2. Regarding OCM mode, the few orbit control manoeuvres that have been needed (including a few collision avoidance manoeuvres) to be conducted were successfully conducted. The good thrusters' alignment (based on a dedicated procedure during AIT campaign) allowed a very good value of off-modulation ratio, thus achieving an optimal performance for orbital manoeuvres.

Furthermore, all equipment behaved nominally and the spacecraft has all nominal and redundant chains available to extend the mission for several years.

2.2 Pointing performance

During IOC, nine different observations were performed to assess pointing performances, first without payload in the loop, for different orientations with respect to the anti-sun direction. This characterization was conducted after the original misalignment calibration described in section §3. A mean value of the offset was computed for each direction based on the instrument centroid telemetry, getting the values of 1.17 and 1.54 arcsec for X and Y axis, respectively. These bias values were corrected on-board by a standard star tracker optical heads orientation calibration procedure, in such a way that the central software uses the correct relative orientation between star tracker and instrument (besides thermoelastic deformations which must be estimated by the PSE).

The computed statistics proved that the pointing performance was comparable for all the observations, below the pointing requirement of 4 arcseconds. After this characterization, a similar process was conducted to evaluate performances with PITL. The following table shows the excellent performances achieved with PITL as evaluated in IOC. Similar behaviour has been obtained during the nominal science operations in the 3.5 years of the mission.

Table 1: Pointing performances with payload in the loop

	X [centi-arcs]	Y [centi-arcs]
68%	17	15
95%	55	46
99.7%	73	77

Figure 3 (top) shows estimation of the thermoelastic bias in X and Y direction during a typical series of observations during the scientific phase of the mission. Without the use of the PSE, that error would directly impact pointing performance. The reduction can be up to 20 microradians for some observations. The flat periods correspond to periods without observations (due to slews between target stars, etc). The observed oscillations are due to thermal excursions at orbital period.

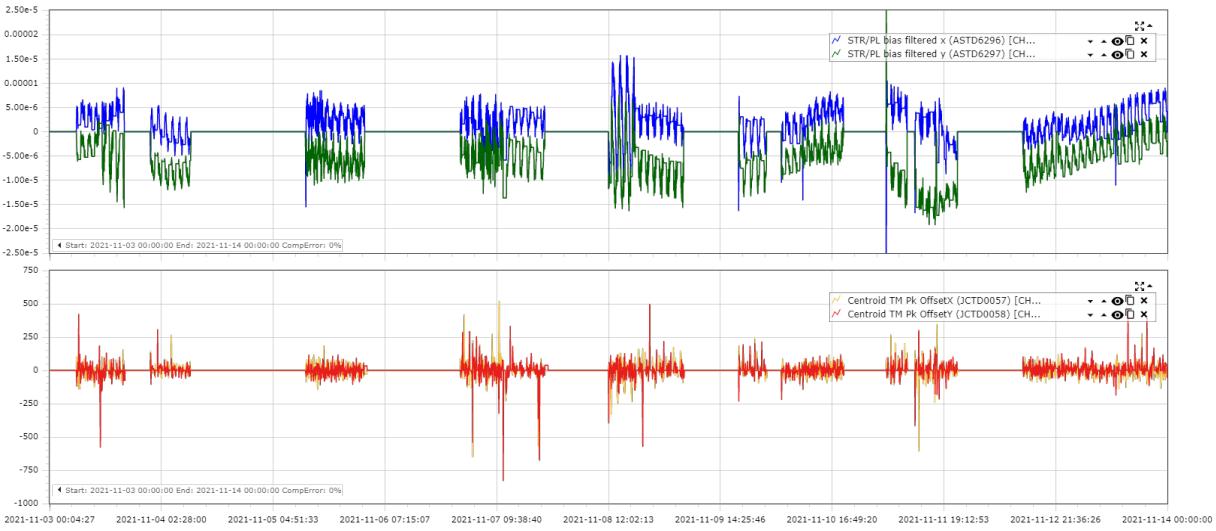

Figure 3. Estimated pointing bias (top, radians) and centroid measurement (bottom, centiarcsec)

The bottom plot shows the centroid position error in CCD frame, as measured by the instrument. The observed values are well below 100 centi-arcseconds for most of the time. Transients are due to slews prior to observation, etc.

3 IN-FLIGHT ALIGNMENT CALIBRATION

3.1 Initial offset calibration strategy

A calibration of the star tracker optical heads orientation was designed to compensate for the misalignment of the instrument line-of-sight due to on-ground measurement errors and launch and zero gravity conditions. This compensation is made through the update of the onboard software parameters related to optical heads orientation with respect the piloting frame.

The instrument line-of-sight is considered to be the center of the CCD. AOCS algorithms have been done in order to be flexible with this definition. The variables Xorig_CCD and Yorig_CCD (available through database), are defined as the raw CCD coordinates of the center of the CCD (thus the instrument LoS) in CCD reference frame. By instrument design, the value of these variables are 51200 centiarcsec for each of them. The piloting reference frame, noted $\boldsymbol{R}_V$, is the one that is used for AOCS control. The AOCS closed-loop tends to align permanently $\boldsymbol{R}_V$ frame with the guidance frame. For that purpose, the star tracker optical heads (STR-OH) measurements are converted from STR-OH reference frame ($\boldsymbol{R}_{OH}$) into $\boldsymbol{R}_V$ frame on-board thanks to STR-OH orientation quaternions from $\boldsymbol{R}_V$ frame to $\boldsymbol{R}_{OH}$ frame.

These star tracker optical heads orientation quaternions are central software parameters computed on-ground after the instrument line-of-sight and optical heads alignment measurement in AIT. But, because of alignment measurement uncertainties and alignment stability (particularly during the launch), the on-ground measurement accuracy may not be compatible with the desired absolute pointing performance. In order to compensate for these uncertainties, a few observations of different stars are done to estimate the absolute instrument line-of-sight alignment bias. The correction of $\boldsymbol{R}_V$ to $\boldsymbol{R}_{OH}$ quaternions on-board, by applying a compensation of the observed bias, allows compensating for this misalignment and improving the absolute pointing performance.

Before calibration, the knowledge of the instrument line of sight reference frame is only estimation. Let us note $\boldsymbol{R}_{Vest}$ the estimated instrument line of sight reference frame, in comparison to $\boldsymbol{R}_V$ which is the real instrument line of sight reference frame. The goal of the calibration procedure is to compute the changing frame quaternion from $\boldsymbol{R}_{Vest}$ to $\boldsymbol{R}_V$ that is the input for a nominal Astrobus procedure that provides the update of the central software value of the star tracker orientation in the AOCS reference frame ($\boldsymbol{R}_{AOCS}$) that corresponds to the instrument line of sight frame ($\boldsymbol{R}_V$).

$$q_{R_{Vest}\,R_V} = [q_0\ q_1\ q_2\ q_3\ ]^T \tag{1}$$

Hence, the operational approach planned to be performed during commissioning was to carry out i observations of different stars with the AOCS estimator working in DSE mode (without PITL) with a TargetLocationX and TargetLocationY (coordinates of the expected position of the target star in the CCD, that can be selected by TC) equal to Xorig_CCD and Yorig_CCD, respectively. Then, with the help of attitude information from star tracker and instrument (J measurements in time for each star) the optimum bias estimation is computed for each observation.

3.2 Computation of optimum bias for one observation

Once one observation is finalized the OffsetX and OffsetY values given by the instrument (not used on-board during calibration) are used to compute the bias. During this one observation there are J measurement of values OffsetX and OffsetY corresponding the difference in centiarcseconds between target position and measured position of star centroid in the CCD. Furthermore there are

available also j measurements of the estimated quaternion from inertial to satellite (piloting) reference frame ${\hat{q}_{R_i\_R_V}}^J$ through DAS packet telemetry, as obtained from the star tracker. Because this telemetry is available at 16 Hz and it is not synchronous to the OffsetX and OffsetY values a filtering process based on a low pass filter over the DSE quaternion error is done to compare both values. This process results on a filtered estimated quaternion, ${\hat{q}^{filt}_{R_{Vest}\_R_{ref}}}^J$. For the sake of simplicity the following notation will be used herein:

$$q_{R_{Vest}\_R_{ref}} = \bar{q}_{DSE\_Rsat\_Ri} \otimes q_{Ref\_Rsat\_Ri} \tag{2}$$

$${\hat{q}^{filt}_{R_{Vest}\_R_{ref}}}^J = \left[q^J_{f0}\ q^J_{f1}\ q^J_{f2}\ q^J_{f3}\right]^T$$

This is the output filtered to be time-synchronous and with similar integration period as the centroid data. On the other hand, the values OffsetX and OffsetY (measured target star centroid offset from nominal location on CCD) can be used to compute the "real" quaternion from satellite reference frame to J2000. Considering the Body 3-2-1 sequence with Euler angles (ϑ_X, ϑ_Y, ϑz) and the following relation between Offset values and rotations about the satellite frame:

$$\alpha_X = \cos^{-1}\left(Y_{Star\ Rsat}\right) - \frac{\pi}{2} \approx -Y_{Star\ Rsat} \approx -\vartheta_Z$$

$$\alpha_Y = \frac{\pi}{2} - \cos^{-1}\left(Z_{Star\ Rsat}\right) \approx Z_{Star\ Rsat} \approx -\vartheta_Y \tag{3}$$

with the following definitions (and noting that LOS_{STAR} is meant to point towards the target star):

- ϑ_Z the angle around Z_{SAT} (first rotation)
- ϑ_Y the angle around Y_{SAT} (second rotation)
- α_X the value of the OffsetX, that is defined as the angle from the XZ_{SAT} plane to the star direction in satellite reference frame
- α_Y the value of the OffsetY, that is defined as the angle from the XY_{SAT} plane to the star direction in satellite reference frame.

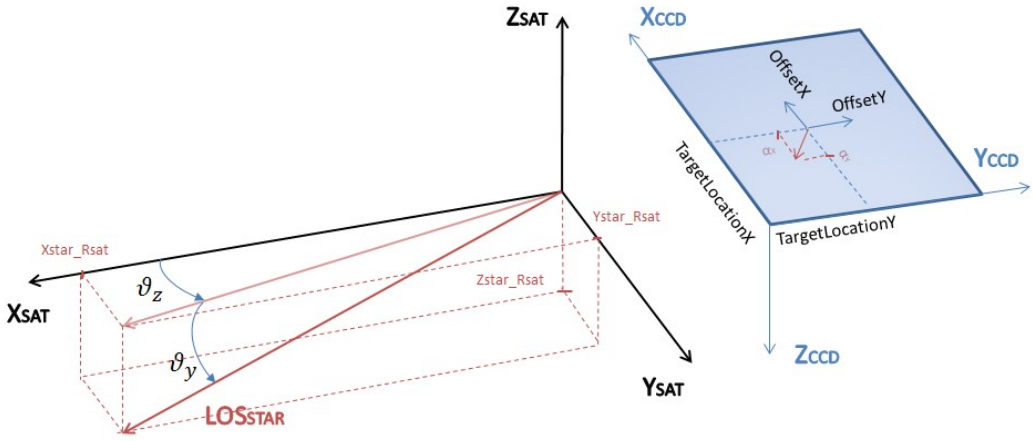

Figure 4. LoS and CCD reference frame definitions

The quaternion from satellite frame real (actual LOS neglecting instrument errors) to a frame with X aligned with LOSstar, and with ϑ_X roll about Xsat. In other words, a frame from the true telescope LOS frame to the desired satellite frame from the guidance can be expressed in terms of OffsetX (α_X) and OffsetY (α_Y) values:

$$\tilde{q}_{R_{Vest}\_R_{ref}}^{real\_des^J} = \begin{bmatrix} \cos(\vartheta_X/2)\cdot\cos(\alpha_Y/2)\cdot\cos(\alpha_X/2) + \sin(\vartheta_X/2)\cdot\sin(\alpha_Y/2)\cdot\sin(\alpha_X/2) \\ \sin(\vartheta_X/2)\cdot\cos(\alpha_Y/2)\cdot\cos(\alpha_X/2) - \cos(\vartheta_X/2)\cdot\sin(\alpha_Y/2)\cdot\sin(\alpha_X/2) \\ -\cos(\vartheta_X/2)\cdot\sin(\alpha_Y/2)\cdot\cos(\alpha_X/2) - \sin(\vartheta_X/2)\cdot\cos(\alpha_Y/2)\cdot\sin(\alpha_X/2) \\ -\cos(\vartheta_X/2)\cdot\cos(\alpha_Y/2)\cdot\sin(\alpha_X/2) + \sin(\vartheta_X/2)\cdot\sin(\alpha_Y/2)\cdot\cos(\alpha_X/2) \end{bmatrix} \approx \begin{bmatrix} 1 \\ \vartheta_X/2 \\ -\alpha_Y{}^J/2 \\ -\alpha_X{}^J/2 \end{bmatrix} \tag{4}$$

where small angle approximation has been used neglecting second order terms. For each instrument measurement j within an observation, we can obtain the conversion quaternion from $\boldsymbol{R}_{Vest}$ to $\boldsymbol{R}_V$:

$$\hat{q}_{R_{Vest}\_R_V}{}^J = \begin{bmatrix} q_{f0}^J \\ -q_{f1}^J \\ -q_{f2}^J \\ -q_{f3}^J \end{bmatrix} \otimes \begin{bmatrix} 1 \\ \frac{\vartheta_X}{2} \\ \frac{-\alpha_Y{}^J}{2} \\ \frac{-\alpha_X{}^J}{2} \end{bmatrix} = \begin{bmatrix} q_{f0}^J + q_{f1}^J\cdot\vartheta_X/2 - q_{f2}^J\cdot\alpha_Y{}^J/2 - q_{f3}^J\cdot\alpha_X{}^J/2 \\ q_{f0}^J\cdot\vartheta_X/2 - q_{f1}^J + q_{f2}^J\cdot\alpha_X{}^J/2 - q_{f3}^J\cdot\alpha_Y{}^J/2 \\ -q_{f0}^J\cdot\alpha_Y{}^J/2 - q_{f2}^J - q_{f3}^J\cdot\vartheta_X/2 - q_{f1}^J\cdot\alpha_X{}^J/2 \\ -q_{f0}^J\cdot\alpha_X{}^J/2 - q_{f3}^J + q_{f1}^J\cdot\alpha_Y{}^J/2 + q_{f2}^J\cdot\vartheta_X/2 \end{bmatrix} \tag{5}$$

It must be noted that all previous variables are known except ϑ_X because the instrument measurements only provides the star direction in satellite frame but is not able to provide the rotation around that axis. The following system of equation can be written for each measurement:

$$\begin{bmatrix} q_{f0}^J + q_{f1}^J\cdot\vartheta_X/2 - q_{f2}^J\cdot\alpha_Y{}^J/2 - q_{f3}^J\cdot\alpha_X{}^J/2 \\ q_{f0}^J\cdot\vartheta_X/2 - q_{f1}^J + q_{f2}^J\cdot\alpha_X{}^J/2 - q_{f3}^J\cdot\alpha_Y{}^J/2 \\ -q_{f0}^J\cdot\alpha_Y{}^J/2 - q_{f2}^J - q_{f3}^J\cdot\vartheta_X/2 - q_{f1}^J\cdot\alpha_X{}^J/2 \\ -q_{f0}^J\cdot\alpha_X{}^J/2 - q_{f3}^J + q_{f1}^J\cdot\alpha_Y{}^J/2 + q_{f2}^J\cdot\vartheta_X/2 \end{bmatrix} \otimes \begin{bmatrix} q_0 \\ q_1 \\ q_2 \\ q_3 \end{bmatrix} = N \tag{6}$$

where N is the quaternion error due to the noise of the measurement. In order to obtain the optimum bias rotation from $\boldsymbol{R}_{Vest}$ to $\boldsymbol{R}_V$ considering all the payload measurements we minimize a cost function defined as the sum of the quadratic angular error of the measurements.
The angular error of each measurement is computed as:

$$\varepsilon_J = 2\cdot\cos^{-1}\left(\left[A_0^J + q_{f1}^J\cdot\vartheta_X\right]\cdot q_0/2 + \left[A_1^J + q_{f0}^J\cdot\vartheta_X\right]\cdot q_1/2 + \left[A_2^J - q_{f3}^J\cdot\vartheta_X\right]\cdot q_2/2 + \left[A_3^J + q_{f2}^J\cdot\vartheta_X\right]\cdot q_3/2\right) \tag{7}$$

where the A^j parameters are functions of parameters q_f and the Euler angles referred above.

Assuming that the angular error is a small angle, previous expression can be simplified to:

$$\varepsilon_J^2 \approx 16\frac{1 - \left[A_0^J + q_{f1}^J\cdot\vartheta_X\right]q_0 - \left[A_1^J + q_{f0}^J\cdot\vartheta_X\right]q_1 - \left[A_2^J - q_{f3}^J\cdot\vartheta_X\right]q_2 - \left[A_3^J + q_{f2}^J\cdot\vartheta_X\right]q_3}{1 + \left[A_0^J + q_{f1}^J\cdot\vartheta_X\right]q_0 + \left[A_1^J + q_{f0}^J\cdot\vartheta_X\right]q_1 + \left[A_2^J - q_{f3}^J\cdot\vartheta_X\right]q_2 + \left[A_3^J + q_{f2}^J\cdot\vartheta_X\right]q_3} \tag{8}$$

The cost function is then

$$f(q_0, q_1, q_2, q_3, \vartheta_X) = \sum_J \varepsilon_J^2 \tag{9}$$

As there were some simplifications during the development of these equations we will impose the norm of the quaternion to be equal to 1 as a constraint to the optimization problem.

$$g(q_0, q_{1,} q_2, q_3) = q_0^2 + q_1^2 + q_2^2 + q_3^2 - 1 \tag{10}$$

Using the method of Lagrange multipliers for solving the optimization problem we obtain the following function:

$$\Lambda(q_0, q_{1,} q_2, q_3, \vartheta_X, \lambda) = f(q_0, q_{1,} q_2, q_3, \vartheta_X) + \lambda \cdot g(q_0, q_{1,} q_2, q_3) \tag{11}$$

And the solution is given by:

$$\nabla_{q_0, q_{1,} q_2, q_3, \vartheta_X, \lambda} \Lambda(q_0, q_{1,} q_2, q_3, \vartheta_X, \lambda) = 0 \tag{12}$$

When differencing this equation, it provides a set of five equations to solve the five state variables: (q_0, q_1, q_2, q_3, ϑ_X). Note that there is also the constraint equation and the Lagrange multiplier that makes a total of 6 variables with 6 equations that has to be solved numerically.

3.3 Calibration execution at IOC

The calibration of the star trackers was prepared to be conducted following the procedure described above, right after the first light observations from the instrument. However, after cover opening, it was found that the star HD 70843 that was targeted to be observed was not in the 1024 x 1024 window of observation. Instead, some other stars close to that one in the field of view were observed to be rotating around a point outside the window, where the target star was actually located. The reason for this is that the misalignment between star tracker reference frame and instrument line of sight reference frame was higher than the width of the window. The calibration procedure explained in previous subchapter assumes that the centroid measurement of the target star is in the CCD reference frame. As this information was not available, some indirect computation were performed to solve this problem.

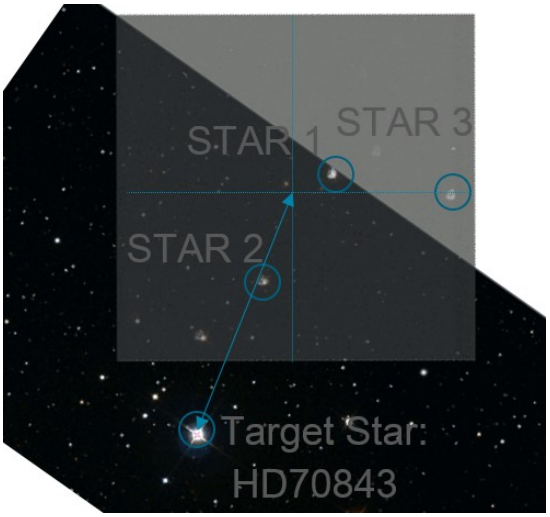

Figure 5. Geometry of the CCD at a certain time at first light

The idea was to estimate the needed data from three bright stars that were identified in the image, i.e. pixel position in CCD and the corresponding value of Right Ascension and Declination at three

different positions (different time). As the target LOS in (RA, Dec) was known, the position in CCD pixels reference frame was obtained as a bilinear interpolation based on the three identified stars. When applying the bilinear interpolation and the optimization procedure described above, the computed values for the offset obtained were (XLoS = -317; YLoS = -723) arcseconds.

After correcting for this deviation a second observation of the same star was performed being the target star this time was very close to the center of the CCD, with a remaining deviation of less than 5 arcseconds as observed in the subsequent plot of the offset reported by the instrument centroid telemetry. A video of downlinked payload imagery was prepared by the science team, which demonstrated the expected behaviour. The target star stayed still in the center of the CCD while the rest of the sky was rotating around it with an average period of the orbital pulsation.

4 EARTH OCCULTATION

Because of the scientific characterization process of exoplanets, for most stars acquisitions the observations periods are longer than CHEOPS orbital period. In these cases, depending on the inertial pointing, there could be some instrument occultation periods with the Earth. This issue was known during the design phase and the strategy was to keep inertial pointing. In the case of not using PITL during the observation (an option that can be selected by operator via a flag in the acquisition command sequence) the satellite would basically keep the same guidance and control behaviour. It should be noted that the occultation is on the instrument, since the star tracker optical heads are not blinded by design in any possible observation attitude. In case the instrument is selected to be used in the AOCS control loop, the instrument would tag as invalid the offset value, so AOCS would not consider that measurement in the control loop and therefore the same behaviour as without PITL was expected.

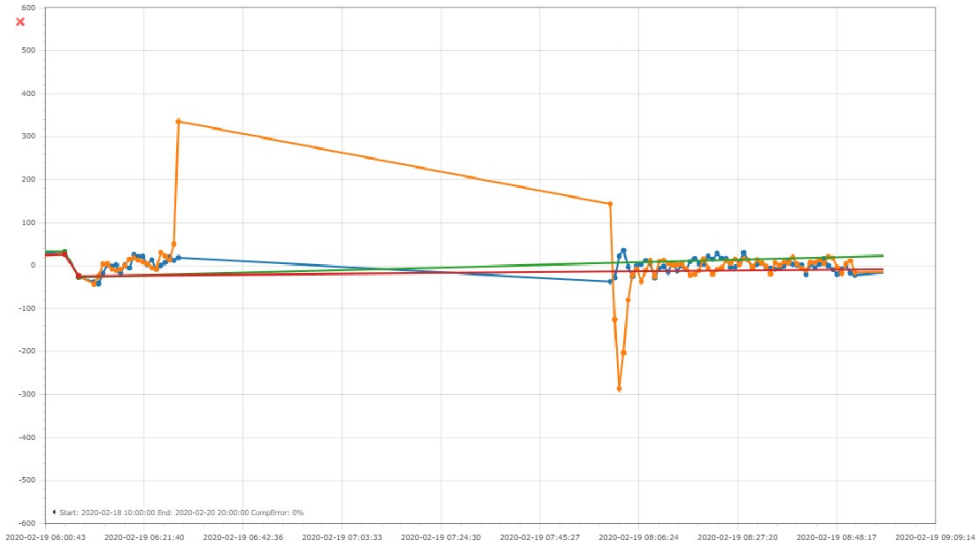

Figure 6. Offset (centi-arcs) detected by instrument before and after an occultation

However, when analyzing data taken for target acquisition with occultation periods and especially when the instrument was providing measurements at high rate, some stars that were properly tracked before the occultation provided a big error attitude when entering and exiting the Earth occultation period. Figure 6 provides the evolution of the offset as observed by the instrument optics - in between the centroids are invalid- for an observation of 2020-02-19. It was found that the star moves in the CCD just before and after occultation by the Earth. The expected behaviour was

that it would keep within PITL precision before the occultation and remain within no PITL during occultation, with slight deviation in terms of performance. Furthermore, it can be observed that regardless the entering and exiting issue, the AOCS good performances (below 1 arcsec in this observation) are recovered.

The smearing of the observed images and the evolution of the offset telemetry first suggested that an abnormal issue of the platform was at the root cause of the observed behaviour. However, the behaviour of the star trackers was checked to be in order. The root cause of this strange behavior just after and before the Earth occultation was quickly discovered afterwards: the atmospheric refraction of the star light in the transition through the Earth atmosphere. The atmosphere deviates the light of the star from a straight line due to the variation in air density as a function of height. This refraction is due to the variation of velocity of light with increased air density (the refractive index increases). This phenomenon has been confirmed also from similar effects observed from ground based astronomy when pointing nearly the local horizon. Such refraction caused the light of the star to quickly evolve within the CCD window, which led to the centroid offset telemetry to evolve accordingly.

The instrument software was not able to distinguish the refraction impact and therefore it still provided to AOCS estimation algorithm some measurements tagged as valid. Therefore, at the beginning of the occultation it causes a shift in the centroid information that leads to an artificial estimation error and causing the platform to react to correct it. The observed phenomenon is visually described in figure 7.

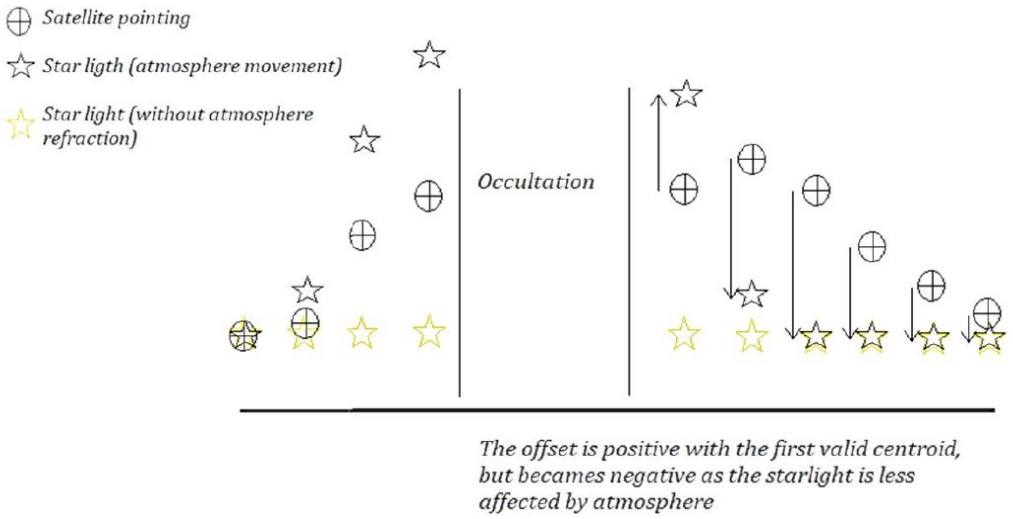

Figure 7. Refraction impact on instrument measurement

At the end of the occultation, the satellite is still depointed with respect to the reality as the misleading centroid information is still considered in the low pass filter for bias correction. In this period there was some need to realign the bias estimation with the actual thermoelastic deformation. These effects can be seen in the centroid offsets, with the convergence quickly achieved as atmospheric is no longer in the field of view of the instrument.

Two counter-measurements were considered to mitigate the problem and to avoid loss of stars. One at AOCS level, limiting the threshold to accept the offset values from the instrument. This avoids big errors introduced in the pointing and therefore always making possible to recover. The second one at instrument level to detect and tag as invalid the data that is actually misleading.

5 ONBOARD TIME MANAGEMENT WITHOUT GPS RECEIVER

The standard implementation of the AS250 platform uses the Airbus DS Mosaic GPS for orbit position, velocity and absolute time knowledge. This high quality element provides the satellite state vector with the required accuracy for an Earth observation mission. Nevertheless, in CHEOPS mission the nominal observation mode did not require such accurate knowledge of the orbit to point to a target star, since the pointing is fixed to an inertial reference. However, some AOCS on-board algorithms required a coarse on-board position knowledge. This is managed by doing on-ground orbit determination based on two-way Doppler measurements and uploading the updated state vector to the satellite. MOC performs this process in an autonomous way.

Another effect of not flying a GPS receiver unit is the management of on-board time. Hence, without a GPS receiver driving a 1 second bandwidth synchronisation, the satellite is not able to maintain autonomously a universal time reference (UTC) and then the telemetry packets (science and housekeeping) are time stamped with the internal on board time elapsed counter (OBT). In the same way, Mission Time Line (MTL) is handled by means of the OBT. The science requirement for proper datation of TM in UTC and conversion of TCs to OBT is 0.1second.

On ground, the time correlation mechanism of the Mission Control System (MCS) takes care of the transformation of OBT to UTC (based on a simple linear trend model) for TM time-stamping (and vice-versa for MTL uplinks). From this point of view, the spacecraft is autonomous and OBT could have been simply left running in free mode over the whole mission lifetime. However, in order to compute the transformation between Earth Center Frame ECEF and J2000 the spacecraft requires absolute knowledge of universal time (UTC) on-board. Such information is needed for Earth magnetic field estimation, OCM manoeuvres and to continuously compute the roll angle to keep instrument radiator away from Nadir direction, thus optimizing instrument thermal stability.

This issue was solved with a linear operational mechanism that took advantage of an already available time correction algorithm in the onboard navigation function from AS250. In Earth observation programs, precise pointing requirements leads to then accurate knowledge of UT1 on-board. The algorithm provides a linear estimation of the UT1 value as function of the OBT (that is synchronized to TAI or UTC reference):

$$UT1 = AOBT2UT1 + (1 + BOBT2UT1) * UTC \tag{13}$$

The parameters (AOBT2UT1; BOBT2UT1) i.e. the time correlation coefficients (offset and slope) that are regularly estimated on ground have to be uplinked to the spacecraft through service 140 commanding (whenever the correlation coefficients change significatively).

For CHEOPS, the same algorithm is applied considering now that the correlation coefficients refers to the conversion from OBT to UTC.

$$UTC = AOBT2UT1 + (1 + BOBT2UT1) * OBT \tag{14}$$

The offset value is initially tuned to zero as at launch pad the OBT is synchronized to UTC. The slope value is initially set to zero too. Before launch, Airbus studied the linear and non-linear effects that would affect to the internal OBC oscillator. The output is that there are two main contributions for the difference between OBT and UTC. The first one is the frequency shift (setting error and long term drifts) of the on-board oscillator with respect the reference GPS oscillator. This constant difference leads to a linear variation in OBT-UTC difference with the elapsed time. The maximum

value (worst case) of this variation is 10ppm, i.e. a slope of 10^{-5}. The second is due to short term effects. The onboard computer (OBC) oscillator has an absolute setting error less than 10^{-5} and a frequency stability better than $25 \cdot 10^{-6}$/day (25 ppm) including all parameters influencing the stability (e.g. ageing, temperature …) on the whole OBC range of temperature (-20ºC to 50ºC). If the temperature range is reduced to 10ºC to 34ºC the stability is better than $3 \cdot 10^{-6}$ (3 ppm) (worst case).

On ground, the MCS provided a set of time couples (TCO, packet SPID 98) of UTC with the correspondent OBT for each pass. The parameters reporting the OBT are extracted for the whole pass with a script, then filtered to remove outliers and finally with a mean square estimation offset and gradient values (AOBT2UT1, BOBT2UT1) are obtained.

5.1 LEOP behaviour

At beginning of LEOP, during ASH mode, the temperature of the OBC (and thus the oscillator) were not controlled, as the thermal control mode was SAFE and the control thresholds were higher. Figure 8 shows the oscillator temperature evolution at beginning of LEOP. It can be observed that the temperature was going down until 18/12/20-21:00 [UTC], moment when thermal control was set to OPERATIONAL, and the OBC heater started to switch on.

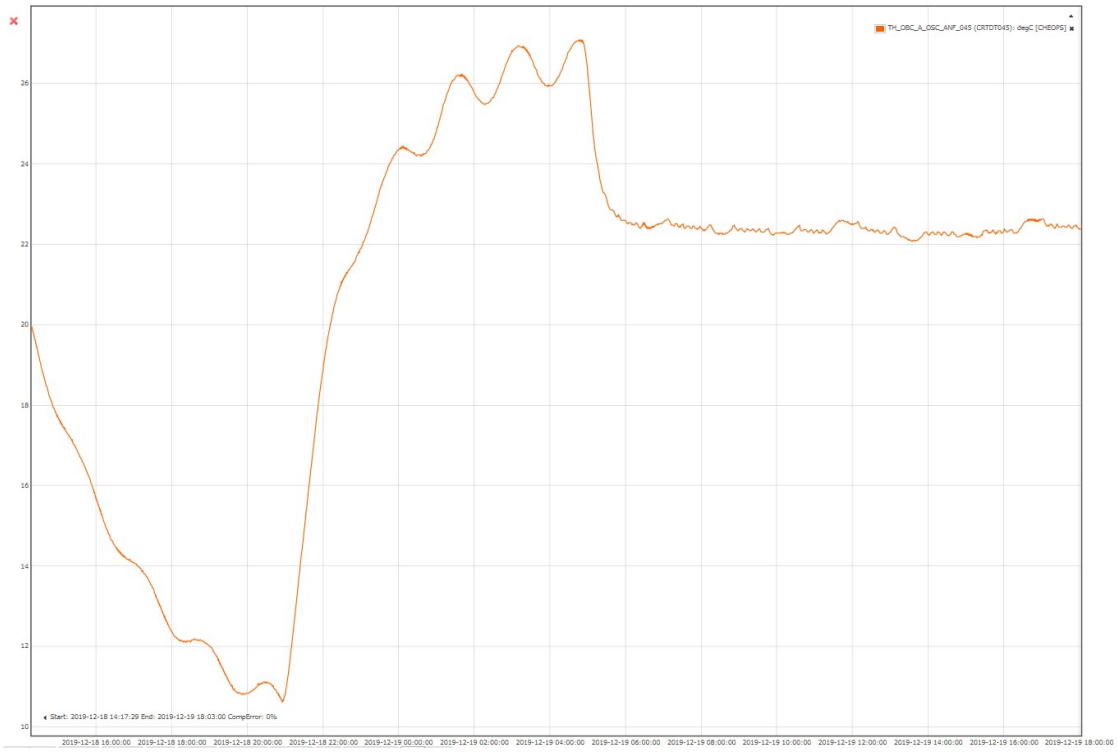

Figure 8. OBC oscillator temperature (ºC) evolution at beginning of LEOP

It was afterwards realized that the thermal drop between the control thermistor of the OBC and the oscillator was about 5º, and that temperature difference would prevent the heater from switching. The thermal controller limit values for the control thermistor were changed to [16º-17º] for the control thermistor and then the OBC temperature started to cycle. This was done on 19/12/2019. From this time on, the temperature of the oscillator was converged to a value between 22º and 23º. Figure 9 shows the UTC to OBT difference based on TCOs at the beginning of LEOP. It can be observed the correspondence between the slope of the OTB-UTC difference and the oscillator temperature. As the temperature goes lower at the beginning, the slope of the time difference

increases, being this slope zero at the time when the temperature crosses the 22 degrees. After that, as the temperature still increased, the slope of the time difference was negative, compensating only after the correct setting of temperature thresholds of the OBC.

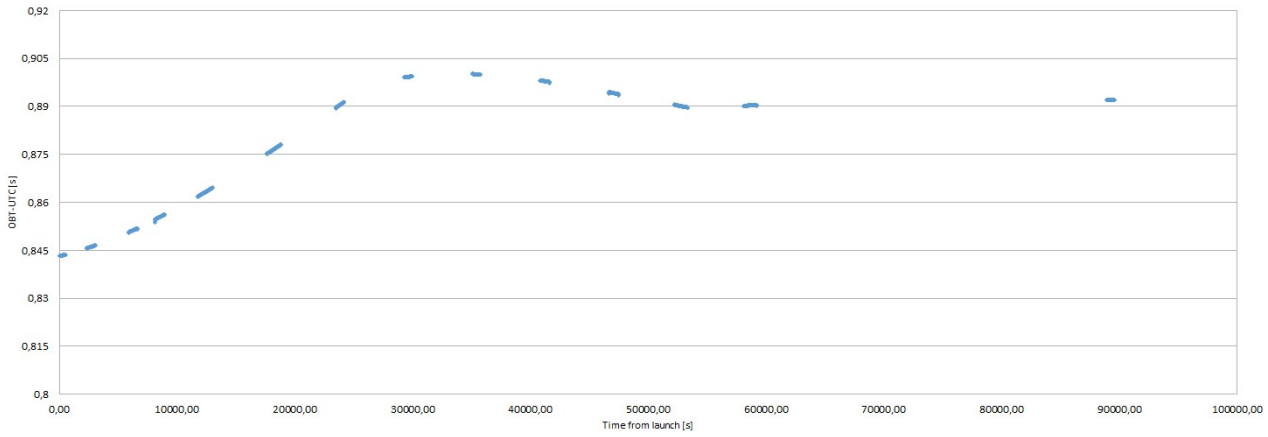

Figure 9. UTC-OBT difference (seconds) evolution during first day in orbit

5.2 IOC behaviour and nominal operations

There was a stand-by period from end of LEOP (22-Dec) until start of IOC (08-Jan) when the satellite was in Sun Pointing (SUP) submode and the instrument was kept switched off. During this period, the gradient of the time difference between OBT and UTC was computed and proved that the assumption of a linear evolution for the OBT drift is correct. The gradient computed until start of IOC (day 20) was $2.5e^{-7}$.

Afterwards the instrument was switched on and from this day a slight reduction of the slope was observed. Once at IOC, and after instrument was switched on, the global temperatures of the platform slightly changed to accommodate with the new dissipations.

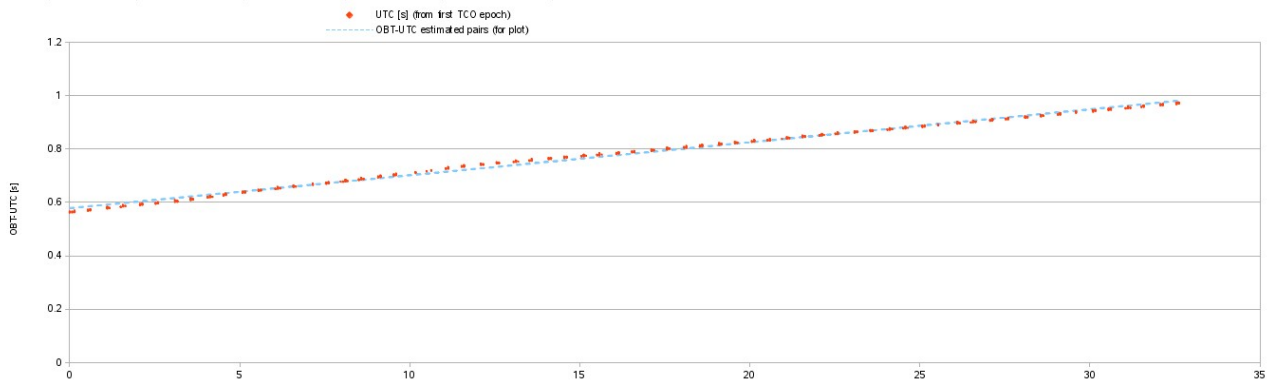

Figure 10. UTC-OBT difference (seconds) after instrument switch-on (horizontal axis in days)

Figure 10 shows the OBT-UTC difference between 23 days in IOC, beginning Jan 23, 2020. The red points show the measured OBT-UTC difference while the blue line shows the best linear estimation. The small temperature change due to the instrument switch on led to slight change in the drift slope. The gradient is now about $1.5e^{-7}$.

As an operational approach for nominal life, it was recommended to SOC to follow the same approach as for with the navigation function. That is to leave the gradient forced, so the automatic process of the MCS only recomputes the offset of the OBT-UTC drift whenever the thresholds are

overpassed. This approach was successfully tested at end of IOC and has been used during operational lifetime.

In case the gradient change during lifetime due to temperature environment, the impact would be that the frequency of update of the constant would be higher. The assessment process has been continued during nominal life of the satellite, and the constant remains valid within 0.02 seconds for more than 20 days. An automatic check in order to prevent sending wrong data to the satellite is already implemented in automation system. Figure 11 shows the residual error as estimated on ground by using the time couples obtained in the ground segment. It can be seen the very good accuracy of the time estimation by using this procedure.

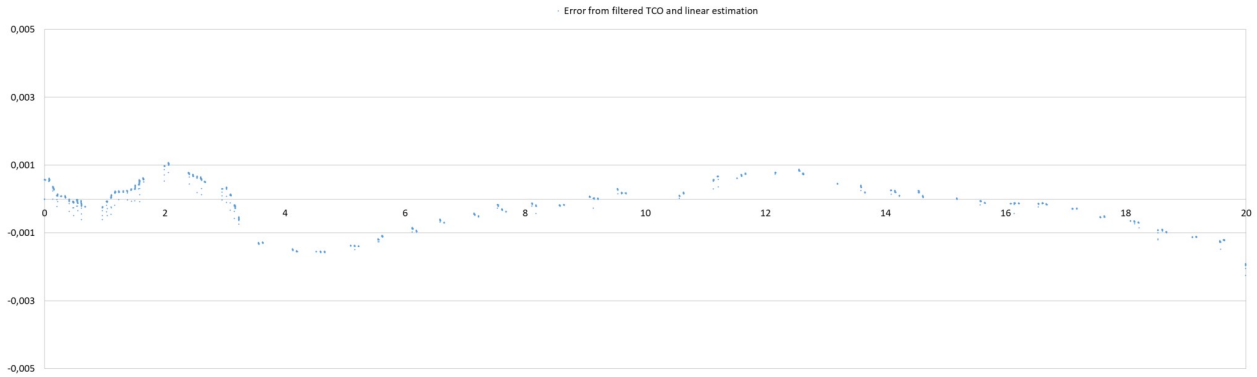

Figure 11. Time estimation error (seconds) at end of IOC (horizontal axis in days)

6 CONCLUSION

The AOCS for CHEOPS mission has remarkably satisfied in-flight all the specified performances, with excellent behaviour in terms of pointing accuracy, robustness, and reliability. The use of payload in the loop has been of paramount relevance to meet the APE requirements well below the specified values, with important contribution to the prominent scientific return. The design has behaved as expected including key items such as safe mode and orbit control manoeuvres. The management of time by means of ground segment support has been properly characterized and set into automatic updates, which in combination with Doppler measurements for state vector updates, allowed the mission not to embark a GPS receiver. Pointing characterization in IOC led to manage unforeseen events such as line of sight deviation due to atmospheric refraction and instrument assembly misalignment higher than initially expected. In summary, after 3.5 years, AOCS keeps highly contributing to the success of this first S-mission in the ESA Science Program.

7 REFERENCES

[1] Benz, W., Broeg, C., Fortier, A. et al. *The CHEOPS mission*. Exp Astron 51, 109–151 (2021).

[2] Borges, A., Montes, T., Cortes, D.,: *CHEOPS mission: A low cost platform for Science*. 10th IAA Symposium on Small Satellites for Earth Observation (Berlin, April 2015)

[3] López-Pina, A., Pizarro, A., Torres, L.,: *Adaptation of an Earth Observation AOCS to an exoplanet characterization mission.* 10th IAA Symposium on Small Satellites for Earth Observation (Berlin, April 2015)